European Journal of Chemistry 2 (2) (2011) 178-188

European Journal of Chemistry

Journal homepage: www.eurjchem.com

Spectroscopic and biological activity studies on tridentate Schiff base ligands and their transition metal complexes

Hanan Farouk Abd El-Halim[a,*], Mohamed Mohamed Omar[b], Gehad Genidy Mohamed[b] and Mohsen Abou El-Ela Sayed[c]

[a] *Pharmaceutical Chemistry Department, Faculty of Pharmacy, Misr International University, Cairo, Heliopolis, 11341, Egypt*
[b] *Chemistry Department, Faculty of Science, Cairo University, Giza, 12613, Egypt*
[c] *Department of Botany, Faculty of Science, Cairo University, Giza 12613, Egypt*

**Corresponding author at: Pharmaceutical Chemistry Department, Faculty of Pharmacy, Misr International University, Cairo, Heliopolis, 11341, Egypt. Tel.: +202.33477280; fax: +202.27953726. E-mail address: hanan_farouk1@hotmail.com (H.F.A. El-Halim).*

ARTICLE INFORMATION

Received: 08 August 2010
Received in revised form: 05 January 2011
Accepted: 05 January 2011
Online: 30 June 2011

KEYWORDS

Schiff bases
Transition metal complexes
Spectral studies
Thermal analyses
Biological activity
Potentiometric measurements

ABSTRACT

Schiff base ligands are prepared via condensation of pyridine-2,6-dicarboxaldehyde with 2-aminothiophenol (H_2L^1) and 2-aminobenzoic acid (H_2L^2), respectively. The ligands are characterized based on elemental analysis, mass, IR and ^1H NMR spectra. Metal complexes are reported and characterized based on elemental analyses, IR, ^1H NMR, solid reflectance, magnetic moment, molar conductance, and thermal analyses (TG, DTG and DTA). The molar conductance reveals that all the metal chelates are non-electrolytes except Th(IV) H_2L^2 complex which is 1:1 electrolyte . IR spectra show that H_2L^1 and H_2L^2 ligands behave as neutral tridentate ligands and bind to the metal ions via the two azomethine N and pyridine N. From the magnetic and solid reflectance spectra, it is found that the geometrical structures of these complexes are octahedral (Cr(III)- and Fe(III)-H_2L^1 and H_2L^2, Th(IV)-H_2L^2 and Mn(II)-H_2L^1 complexes) and triagonal bipyramidal (Co(II), Ni(II), Cu(II), Cd(II) and UO_2(II)-H_2L^1 and H_2L^2 and Mn(II)-H_2L^2 complexes). The thermal behaviour of these chelates is studied using TG and DTA techniques and the activation thermodynamic parameters are calculated using Coats-Redfern method. The synthesized ligands and their metal complexes were screened for their biological activity against bacterial species (*Escherichia coli*, *P. vulgavis*, *B. subtilis* and *S. pyogones*) and fungi (*F. solani*, *A. niger* and *A. liavus*). The activity data show that the metal complexes have antibacterial and antifungal activity more than the parent Schiff base ligands against one or more bacterial or fungi species.

1. Introduction

The preparation of a new ligand was perhaps the most important step in the development of metal complexes which exhibit unique properties and novel reactivity. Since the electron donor and electron acceptor properties of the ligand, structural functional groups and the position of the ligand in the coordination sphere together with the reactivity of coordination compounds may be the factor for different studies [1]. Schiff bases are an important class of ligands, such ligands and their metal complexes had a variety of applications including biological, clinical, analytical and industrial in addition to their important roles in catalysis and organic synthesis [2-5]. In early work closely related to the system of interest here, Lions and Martin [6] synthesized Schiff base ligands from 2,6-pyridinedicarboxaldehyde (PDC) with aniline and benzylamine and noted that the free ligands were crystalline materials. Therefore, studies ensued in which this same pair of Schiff base linkages was incorporated in many different kinds of polydentate ligands, including various macrocyclic ligands [7,8]. Pursuing the analogy to the Sauvage template, *p*-aminophenol was used as the amine in the straightforward Schiff base condensation reaction with PDC to give the diphenolic ligand. Previous studies on ligands and metal complexes derived from the Schiff bases of *o*- and *p*-aminophenol are few. In one case, the reaction between PDC and *o*-, *m*- and *p*-aminophenols in the presence of cadmium ions was used to differentiate aminophenol isomers [9] and *p*-aminophenol had appeared in some recent publications as a Schiff base precursor. Two of these studies examined hydrogen-bonding interactions of the phenolic hydrogen [10] while another involved estrification of the phenolic oxygen of the free Schiff base ligand to construct potential metallomesogen components [11]. The X-ray crystal structure of L^1 and its Ni (II) and Zn (II) complexes had been reported by Vance *et al.* [12]. Metal and mixed ligand complexes of L^1 and L^2 ligands have been reported [13,14]. The structures of these ligands are shown in Figure 1. Therefore, in continuation to our interest in Schiff base ligands and their metal chelates [13-15], this work deals with the synthesis and characterization of Schiff base ligands; H_2L^1 and H_2L^2, and their complexes.

The coordination behaviour of H_2L^1 and H_2L^2 ligands (Figure 2) towards transition metal ions (Fe(II), Co(II), Ni(II), Cu(II) and Zn(II), UO_2(II) and Th(IV)) is investigated via IR, molar conductance, magnetic moment, solid reflectance and thermal analysis. The thermal decomposition of the complexes is also used to infer the structure and different thermodynamic activation parameters are calculated. The biological activity of these Schiff bases and their metal chelates are reported.

ISSN 2153-2249 (Print) / ISSN 2153-2257 (Online)
DOI:10.5155/eurjchem.2.2.178-188.240

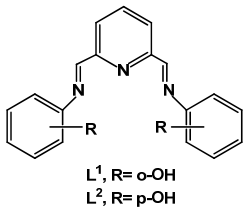

Figure 1. Structure of L^1 and L^2 ligands.

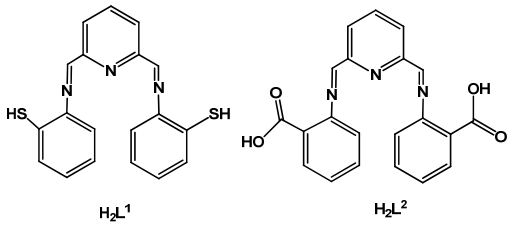

Figure 2. Structure of Schiff bases.

2. Experimental

2.1. Materials and reagents

All chemicals used were of the analytical reagent grade (AR), and of the highest purity available. They included anthranilic acid (Aldrich); 2-aminothiophenol, 2,6-pyridinedicarboxaldehyde (Sigma), $ThCl_4.4H_2O$ (Sigma) and $CdCl_2$ and $CuCl_2.2H_2O$ (Sigma); $UO_2(CH_3COO)_2.2H_2O$ and $FeCl_3.6H_2O$ (Prolabo); $CrCl_3.6H_2O$, $CoCl_2.6H_2O$ and $NiCl_2.6H_2O$ (BDH). Zinc oxide, disodium salt of ethylenediaminetetraacetic acid; EDTA; (Analar), ammonia solution (33%, v/v) and ammonium chloride (El-Nasr Pharm. Chem. Co., Egypt). Organic solvents used included absolute ethyl alcohol, diethylether, and dimethylformamide (DMF). These solvents were spectroscopic pure from BDH. Hydrogen peroxide, sodium chloride, sodium carbonate and sodium hydroxide (AR) were used. Hydrochloric and nitric acids (Merck) were used. De-ionized water collected from all glass equipments was usually used in all preparations.

2.2. Solutions

Fresh stock solutions of $1x10^{-3}$ M ligands; H_2L^1 and H_2L^2 were prepared by dissolving the accurately weighed amounts of H_2L^1 (0.215 g/L) and H_2L^2 (0.219 g/L) in the appropriate volume of absolute ethanol. $1x10^{-3}$ M Stock solutions of the metal salts were prepared by dissolving the accurately weighed amounts of the metal salts in the appropriate volume of de-ionized water. The metal salt solutions were standardized. Dilute solutions of the metal ions and Schiff bases of $2.5x10^{-6}$, $1x10^{-6}$, $2.5x10^{-5}$, $1x10^{-5}$ and $1x10^{-4}$ M were prepared by accurate dilution.

For potentiometric studies, all solutions of metal ions were prepared by dissolving the calculated amount of their salts in the least amount of water, then ethanol was added to the appropriate volume. 0.1 N hydrochloric acid was prepared and standardized using sodium carbonate. 1.0 M sodium chloride solution was also prepared. A 1:1 sodium hydroxide solution was prepared from A.R. product and stored in a well steamed waxed tall glass cylinder and shacked well for some days to obtain a carbonate free sodium hydroxide solution.

2.3. Instrumentations

pH measurements were carried out using 716 DMS Titrino Metrohm connected with 728 Metrohm Stirrer. Elemental microanalyses of the separated solid chelates for C, H, N and S were performed in the Microanalytical Center, Cairo University. The analyses were repeated twice to check the accuracy of the results obtained. The molar conductance of solid chelates in DMF was measured using Sybron-Barnstead conductometer (Meter-PM.6, E = 3406). Infrared spectra were recorded on a Perkin-Elmer FT-IR type 1650 spectrophotometer in wave number region 4000-400 cm^{-1}. The spectra were recorded as KBr pellets. The solid reflectance spectra were measured on a Shimadzu 3101pc spectrophotometer. The molar magnetic susceptibility was measured on powdered samples using the Faraday method. The diamagnetic corrections were made by Pascal's constant and $Hg[Co(SCN)_4]$ was used as a calibrant. The mass spectra were recorded by the EI technique at 70 eV using MS-5988 GS-MS Hewlett-Packard instrument in the Microanalytical Center, Cairo University. The ^1H NMR spectra were recorded using 300 MHz Varian-Oxford Mercury. The deuterated solvent used was dimethylsulphoxide (DMSO) and the spectra extended from 0 to 15 ppm. The thermal analyses (TG, DTG and DTA) were carried out in dynamic nitrogen atmosphere (20 mL/min) with a heating rate of 10 °C/min using Shimadzu TG-60H and DTA-60H thermal analyzers. The biological activity was carried out at the Microananlytical center, Cairo University.

2.4. Procedures

2.4.1. Potentiometric measurements

The potentiometric measurements were carried out at 25 °C and at ionic strength μ = 0.1 M by addition the appropriate amounts of 1.0 M sodium chloride solution. The pH-meter was calibrated before each titration using standard buffers. The ionization constants of the investigated Schiff bases and the stability constants of their metal chelates with Cr(III), Mn(II), Fe(III), Co(II), Ni(II), Cu(II), Zn(II), Cd(II), Th(IV), and UO_2(II) ions were determined potentiometrically using the technique of Sarin and Munshi [16]. The ionization constants of the ligands are calculated using the equation used by Irving and Rossotti [17]. While metal-ligand stability constants were calculated using methods applied for computing successive stability constants [18].

2.4.2. Synthesis of Schiff bases (H_2L^1 [20], H_2L^2)

A hot solution (60 °C) of 2-aminothiophenol (1.85 g, 14.82 mmol) or 2-aminobenzoic acid (2.44 g, 17.78 mmol) in 25 mL ethanol was mixed with a hot solution (60 °C) of 2,6-pyridinedicarboxaldehyde (1.00 and 1.20 g, 7.41 and 8.89 mmol) for H_2L^1 and H_2L^2, respectively, and the reaction mixture was left under reflux for 4 h. The formed solid product was separated by filtration, purified by crystallization from ethanol, washed with diethyl ether and dried under vacuum over anhydrous calcium chloride. The yellow Schiff base products; H_2L^1 and H_2L^2, were produced in 85 and 87% yield, respectively.

2.4.3. Synthesis of metal complexes

The metal complexes of the Schiff bases were prepared by the addition of a hot solution (60 °C) of the appropriate metal chloride or acetate (1 mmol) in an ethanol-water mixture (1:1, 25 mL) to a hot ethanolic solution (60 °C) of the Schiff bases (0.30 g H_2L^1 or H_2L^2; 25 mL). The resulting mixture was stirred under reflux for 1 h whereupon the complexes were precipitated. They were collected by filtration, washed several times with an ethanol-water mixture (1:1) and diethyl ether. The analytical data for C, H and N were repeated twice.

2.4.4. Determination of the metal content of the chelates

The metal contents were determined complexometrically by titration against standard EDTA solution at a suitable pH value using the suitable indicator.

2.5. Biological activity

Antimicrobial activity of the tested samples was determined using a modified Kirby-Bauer disc diffusion method [20]. 100 µL of the tested bacteria or fungi were grown in 10 mL of fresh media until they reached a count of approximately 108 cells/mL for bacteria and 105 cells/mL for fungi [21]. 100 µL of microbial suspension was spread onto agar plates corresponding to the broth in which they were maintained. Isolated colonies of each organism that might be playing a pathogenic role should be selected from primary agar plates and tested for susceptibility by disc diffusion method [22]. Of the many media available, NCCLS recommends Mueller-Hinton agar due to it results in good batch-to-batch reproducibility. Disc diffusion method for filamentous fungi tested by using approved standard method (M38-A) developed [23]. For evaluating the susceptibilities of filamentious fungi to antifungal agent, plates inoculated with filamentous fungi as asprgillus flavus at 25 °C for 48 h were prepared. Gram (+) bacteria as *Staphylococcus aureus* and Gram(-) bacteria as *Escherichia coli* were incubated at 35-37 °C for 24-28 h. Yeast as *Candida albicans* was also incubated at 30 °C for 24-28 h. The diameters of the inhibition zones were measured in millimeters [24]. Standard discs of tetracycline (antibacterial agent), and amphotericin B (antifungal agent) served as positive controls for antimicrobial activity but filter discs impregnated with 10 µL of solvent (distilled water, chloroform, DMSO) were used as a negative control. The agar used is Meuller-Hinton agar that is rigorously tested for composition and pH. Further the depth of the agar in the plate is a factor to be considered in the disc diffusion method. This method is well documented and standard zones of inhibition have been determined for susceptible and resistant values. Blank paper disks (Schleicher and Schuell, Spain) with a diameter of 8.0 mm were impregnated with 10 µL of tested concentration of the stock solutions. When a filter paper disc impregnated with a tested chemical is placed on agar, the chemical will diffuse from the disc into the agar. This diffusion will place the chemical in the agar only around the disc. The solubility of the chemical and its molecular size will determine the size of the area of chemical infiltration around the disc. If an organism is placed on the agar, it will not grow in the area around the disc if it is susceptible to the chemical. This area of no growth around the disc is known as zone of inhibition or clear zone. For the disc diffusion, the zone diameters were measured with slipping calipers of the national committee for clinical laboratory standards [25]. Agar based methods such E test and disc diffusion can be good alternatives because they are simpler and faster than broth-based methods [26,27].

3. Results and discussion

3.1. Characterization of Schiff bases

The synthesized Schiff bases are subjected to elemental analyses, mass, IR and ^{1}H NMR spectroscopy. The results of elemental analyses (C, H and N) with molecular formulae and the melting points are presented in Tables 1 and 2. The results obtained are in good agreement with those calculated for the suggested formulae (Figure 2) and the melting point is sharp indicating the purity of the prepared Schiff bases.

3.2. Mass spectra of the Schiff bases

The electron impact mass spectra of H_2L^1 and H_2L^2 ligands are recorded and investigated at 70 eV of electron energy. The mass spectra of the studied Schiff bases are characterized by moderate to high relative intensity molecular ion peaks. The mass spectrum of H_2L^1, and the possible molecular ion peaks with their respective relative intensities are shown in Scheme 1. Fragments at m/z = 187 (R.I. = 100 %, base peak) may be due to $C_{11}H_8NS$ ion. The other molecular ion peaks appeared in the mass spectrum (abundance range from 2-100 %) is attributed to the fragmentation of H_2L^1 molecule obtained from the rupture of different bonds inside the molecule. The mass spectra of H_2L^2 and the molecular ion peaks of the different suggested fragments are shown in Scheme 2. H_2L^2 shows a parent peak at m/z = 373 with a relative intensity = 11 %. Fragment at m/z = 69 (R.I. = 94 %, base peak) is attributed to $C_3H_2O_2$ ion.

3.3. Potentiometric determination of the ionization constants

The ionization constants of the ionizable groups in Schiff bases under investigation are determined by a method similar to that described by Sarin and Munshi [16]. The average of protons associated with the ligand ($\bar{n}_A$) at different pH values is calculated utilizing acid and ligand titration curves. The pK_a values can be calculated from the curves obtained by plotting $\bar{n}_A$ versus pH. The formation curves are found between 0 and 1. This indicates that the ligands have one dissociable proton which is from the SH (ligand H_2L^1) and COOH groups (ligand H_2L^2). The pK_a values of 9.56 (ΔG^o = -54.11 KJ/mol) and 6.81 (ΔG^o = -38.44 KJ/mol) are attributed to the ionization of SH and COOH protons in the ligands, H_2L^1 and H_2L^2, respectively. The free energy change is also calculated and the negative values indicate the spontaneous character of association reaction.

3.4. Potentiometric determination of the stability constants

The stability constants of the Cr(III), Mn(II), Fe(III), Co(II), Ni(II), Cu(II), Zn(II), Cd(II), Th(IV) and UO_2(II) complexes with H_2L^1 and H_2L^2 are determined potentiometrically using the method described by Sari [28] and Bjerrum [29].

The formation curves of the investigated complexes are obtained by plotting a graph between the average number of ligands attached per metal ion ($\bar{n}$) and the free ligand exponent (pL). Values of $\bar{n}$ and pL are calculated. The maximum $\bar{n}$ values calculated for metal-ligand system are found not to exceed two indicating the formation of 1:1 and 1:2 (metal: ligand) complexes. The mean log β_1 and log β_2 values of the Cr(III), Mn(II), Fe(III), Co(II), Ni(II), Cu(II), Zn(II), Cd(II), Th(IV) and UO_2(II) complexes with H_2L^1 and H_2L^2 are listed in Table 3.

The order of stability constants is found to be Zn(II) < Cu(II) > Ni(II) > Co(II) > Mn(II) and Cr(III)> UO_2 = Fe(III) = Th(IV) = Cd(II) in accordance with the Irving and Williams order [30] for divalent metal ions of the 3d series. It is clear from Table 3 that the stability of Cu(II) complexes is considerably larger as compared to other metals of the 3rd series. Under the influence of the ligand field, Cu(II) ($3d^9$) will receive some extra stabilization [31] due to tetragonal distortion of octahedral symmetry in their complexes. The Cu(II) complexes will be further stabilized due to the Jahn-Teller effect [32]. One would expect a bigger difference between log K_1 and log K_2 values in such ligands because possible steric hindrance to the linking of the second ligand to the metal ion. The small difference may be due to trans-structure. The free energy of formation, ΔG^o accompanying the complexation reaction has been determined at 25 °C.

Table 1. Analytical and physical data of H_2L^1 ligand and its complexes.

Compound	Colour (Yield, %)	M.p. (°C)	% Found (Calcd.) C	H	N	S	M	$\mu_{eff.}$ (B.M.)	Λ_m $\Omega^{-1}mol^{-1}cm^2$
H_2L^1	Brown	190	65.68	4.53	12.32	18.90	-	-	-
$C_{19}H_{15}N_3S_2$	(85)		(65.32)	(4.29)	(12.03)	(18.33)			
$[Cr(H_2L^1)(H_2O)_3]Cl_3$	Grey	150	41.02	3.61	7.31	11.12	9.01	4.12	370.00
$C_{19}H_{21}Cl_3CrN_3S_2O_3$	(88)		(40.60)	(3.73)	(7.47)	(11.39)	(9.26)		
$[Mn(H_2L^1)Cl_2]\cdot 2H_2O$	Green	145	44.49	4.12	8.15	12.31	10.56)	3.30	19.56
$C_{19}H_{19}MnCl_2N_3S_2O_2$	(75)		(44.62)	(3.71)	(8.22)	(12.52)	(10.74)		
$[Fe(H_2L^1)(H_2O)_3]Cl_3\cdot H_2O$	black	110	39.45	4.19	7.59	11.52	9.24	5.83	365.00
$C_{19}H_{23}Cl_3FeN_3S_2O_4$	(96)		(39.08)	(3.94)	(7.20)	(10.97)	(9.56)		
$[Co(H_2L^1)Cl_2]\cdot H_2O$	Black	110	45.69	3.25	8.76	13.07	11.63	4.49	13.52
$C_{19}H_{17}Cl_2CoN_3OS_2$	(76)		(45.88)	(3.42)	(8.45)	(12.87)	(11.85)		
$[Ni(H_2L^1)Cl_2]\cdot H_2O$	Green	>300	45.85	3.69	8.36	12.65	11.53	3.73	20.12
$C_{19}H_{17}Cl_2NiN_3S_2O$	(83)		(45.90)	(3.42)	(8.45)	(12.88)	(11.81)		
$Cu(H_2L^1)Cl_2]\cdot 4H_2O$	Black	115	40.93	3.79	7.44	11.76	11.55	2.01	26.18
$C_{19}H_{23}Cl_2CuN_3S_2O_4$	(86)		(41.04)	(4.14)	(7.56)	(11.52)	(11.43)		
$[Cd(H_2L^1)Cl_2]\cdot 4H_2O$	Green	240	37.89	3.66	6.65	10.22	18.33	Diam.	30.04
$C_{19}H_{23}Cl_2CdN_3S_2O_4$	(84)		37.72	(3.80)	(6.94)	(10.58)	(18.59)		
$[UO_2(H_2L^1)(CH_3COO)_2]\cdot H_2O$	Green	120	36.35	3.15	5.43	8.32	31.39	Diam.	22.20
$C_{23}H_{23}N_3S_2O_7U$	(80)		(36.55)	(3.04)	(5.56)	(8.47)	(31.52)		

Table 2. Analytical and physical data of H_2L^2 ligand and its complexes.

Compound	Colour (Yield, %)	M.p. (°C)	% Found (Calcd.) C	H	N	M	$\mu_{eff.}$ (B.M.)	Λ_m $\Omega^{-1}mol^{-1}cm^2$
H_2L^2	Brownish	80	7.34	4.23	11.50	-	-	-
$C_{21}H_{15}N_3O_4$	(80)		(67.56)	(4.02)	(11.26)			
$[Cr(H_2L^2)Cl_3]\cdot 3H_2O$	Grey	50	43.52	3.24	7.34	8.67	4.42	18.50
$C_{21}H_{21}Cl_3CrN_3O_7$	(91)		(43.04)	(3.58)	(7.17)	(8.88)		
$[Mn(H_2L^2)(H_2O)Cl_2]\cdot 3H_2O$	yellowish	150	4.39	4.13	7.67	9.42	3.01	21.52
$C_{21}H_{23}Cl_2MnN_3O_8$	(86)		(44.14)	(4.02)	(7.35)	(9.61)		
$[Fe(H_2L^2)Cl_3]$	Black	>300	7.26	3.10	8.12	10.23	5.51	16.35
$C_{21}H_{15}Cl_3FeN_3O_4$	(86)		(47.07)	(2.80)	(7.84)	(10.42)		
$[Co(H_2L^2)Cl_2]\cdot 2H_2O$	Blue	100	6.54	3.28	7.46	10.21	4.91	14.05
$C_{21}H_{19}Cl_2CoN_3O_6$	(80)		(46.76)	(3.52)	(7.79)	(10.92)		
$[Ni(H_2L^2)Cl_2]\cdot 4H_2O$	Green	190	3.70	3.96	7.55	10.15	3.17	13.73
$C_{21}H_{23}Cl_2N_3NiO_8$	(71)		(43.84)	(4.00)	(7.30)	(10.21)		
$[Cu(H_2L^2)Cl_2]\cdot 3H_2O$	Green	170	5.16	4.01	7.30	11.14	1.96	18.51
$C_{21}H_{21}Cl_2CuN_3O_7$	(84)		(44.87)	(3.73)	(7.47)	(11.30)		
$[Cd(H_2L^2)Cl_2]\cdot 3H_2O$	Yellowish	105	1.56	3.52	6.70	18.35	Diam.	13.63
$C_{21}H_{21}Cl_2CdN_3O_7$	(79)		(41.28)	(3.44)	(6.88)	(18.41)		
$[Th(H_2L^2)Cl_3]Cl$	Brownish	170	3.49	2.31	5.41	31.16	Diam.	95.00
$C_{21}H_{15}Cl_4ThN_3O_4$	(83)		(33.73)	(2.00)	(5.62)	(31.05)		
$[UO_2(H_2L^2)(CH_3COO)_2]\cdot H_2O$	Yellow	>300	8.63	3.13	5.26	30.75	Diam.	20.31
$C_{25}H_{23}N_3O_{11}U$	(83)		(38.51)	(2.95)	(5.39)	(30.55)		

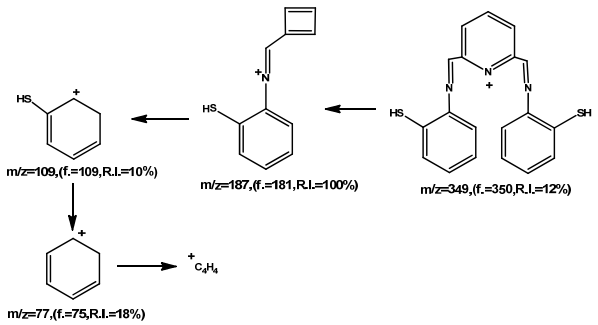

Scheme 1

The results are given in Table 3. From the table, it is apparent that the negative values of ΔG^o show that the driving tendency of the complexation reaction is from left to right and the reaction proceeds spontaneously.

3.5. Composition and structures of Schiff base complexes

Although H_2L^1 [20] ligand is previously prepared but no studies concerning its Cr(III), Fe(III), Cu(II), Cd(II), Th(IV) and UO_2(II) complexes are given. In addition, the stability constants of the metal complexes of and H_2L^1 ligands and thermal stability of metal complexes of H_2L^1 ligand are not previously reported. On screening the literature survey, the biological activities are not studied. So the main target of our work is to prepare the solid complexes of these ligands and carrying out their complete characterization using different physico-chemical techniques together with studying their biological activities. The isolated complexes were subjected to elemental analyses (C, H, N, S and metal content), infrared spectral studies (IR), nuclear magnetic resonance (^{1}H NMR), magnetic studies, molar conductance and thermal analyses (TG, DTG and DTA), to identify their tentative formulae in a trial to elucidate their molecular structures.

Table 3. Cumulative data of log β_1 and log β_2 values for H_2L^1 and H_2L^2 complexes*.

Complexes	log β_1				log β_2				
	A	B	M	-ΔG° (KJ/mol)	A	B	C	M	-ΔG° (KJ/mol)
H_2L^1									
Cr(III)	9.93	10.62	10.27	57.30	19.31	20.03	19.63	19.65	109.6
Mn(II)	9.95	10.65	10.30	57.46	19.36	20.07	19.69	19.70	109.9
Fe(III)	9.91	10.60	10.25	57.19	19.27	19.96	19.58	19.60	109.4
Co(II)	9.96	10.67	10.31	57.52	19.38	20.09	19.71	19.72	110.0
Ni(II)	9.99	10.73	10.36	57.80	19.43	20.13	19.75	19.77	110.3
Cu(II)	10.10	10.76	10.43	58.19	19.52	20.14	19.81	19.82	110.6
Zn(II)	9.98	10.68	10.33	57.63	19.40	20.11	19.72	19.74	110.1
Cd(II)	9.88	10.19	10.03	55.96	19.22	19.53	19.50	19.41	108.3
Th(IV)	9.89	10.20	10.04	56.01	19.24	19.55	19.56	19.45	108.5
UO_2(II)	9.92	10.61	10.26	57.24	19.29	19.98	19.62	19.63	110.0
H_2L^2									
Cr(III)	6.38	7.16	6.77	37.77	12.54	13.17	13.41	13.04	72.8
Mn(II)	6.44	7.18	6.81	37.99	12.63	13.23	13.42	13.09	73.0
Fe(III)	6.33	7.11	6.72	37.49	12.40	13.06	13.39	12.95	72.3
Co(II)	6.45	7.21	6.83	38.10	12.66	13.27	13.43	13.12	73.2
Ni(II)	6.58	7.26	6.92	38.61	12.79	13.37	13.44	13.20	73.7
Cu(II)	6.68	7.36	7.02	39.16	12.89	13.42	13.48	13.26	74.0
Zn(II)	6.54	7.24	6.89	38.44	12.72	13.33	13.45	13.16	73.4
Cd(II)	6.20	6.85	6.52	36.37	11.76	12.47	12.66	12.29	68.6
Th(IV)	6.30	7.08	6.69	37.32	12.33	13.02	13.32	12.89	72.0
UO_2(II)	6.35	7.13	6.74	37.6	12.49	13.12	13.40	13.00	72.6

* (A) Interpolation at half values method, (B) Correction-term method, (C) Mid-point method.

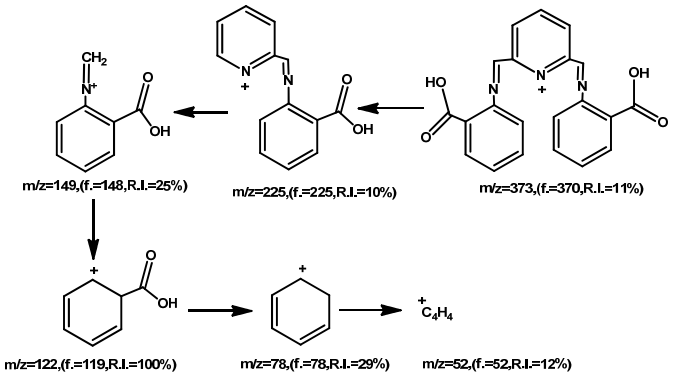

Scheme 2

3.6. Elemental analyses of the complexes

The results of elemental analyses, Tables 1 and 2 are in good agreement with those required by the proposed formulae.

3.7. Molar conductivity measurements

Tables 1 and 2 show the molar conductance values of the complexes. It is found that Fe(III) and Cr(III) chelates have molar conductance values of 365 and 370 Ω^{-1} $mol^{-1}cm^2$ of H_2L^1, respectively. While Fe(III) and Cr(III) chelates of H_2L^2 ligand have molar conductance values of 16.35 and 18.50 Ω^{-1} mol^{-1} cm^2, respectively. This indicates bonding of the chloride anions to the Fe(III) and Cr(III) ions. So, the Fe(III) and Cr(III) chelates are considered as non-electrolytes with H_2L^2 ligand.

On the other hand, the molar conductivity values of Mn(II), Co(II), Ni(II), Cu(II), Zn(II) and Cd(II) chelates of H_2L^1 and H_2L^2 ligands (Λ_m = 13.52 -30.04 Ω^{-1} mol^{-1} cm^2) indicate that these complexes are non-electrolytes. While UO_2(II) complexes of H_2L^1 and H_2L^2 ligands have molar conductivity values of 22.20 and 20.31 $\Omega^{-1}mol^{-1}cm^2$, respectively, which indicates the non-ionic nature of these complexes and hence they are considered as non-electrolytes. Th(IV) complex of H_2L^2 ligand has molar conductivity value 95 Ω^{-1} mol^{-1} cm^2, indicating its ionic nature and of the type 1:1 electrolyte.

3.8. IR spectral studies

H_2L^1 and H_2L^2 Schiff base ligands are of significant interest from the point of view that they act as a pincer ligands, often found as a merdional ligand (i.e. the three nitrogen atoms possess will be approximately coplanar in metal coordination sphere) and exhibited a great variety of coordination modes with different coordinating power and these may give rise to varied bonding and different stereochemical patterns in their coordination complexes as a result for competition between the thiophenolic, carboxylic and azomethine nitrogen groups as a coordination sites [33,34]. The compounds containing a pyridinium moiety attached to a heterocyclic system are important in natural product chemistry and in organic synthesis [35]. This would lead us to obtain some new heterocyclic compounds with expected wide spectrum of potential applications that were extensively required for medicinal chemistry program.

The data of the IR spectra of Schiff base ligands (H_2L^1, and H_2L^2) and their complexes are listed in Tables 4 and 5. The IR spectra of the complexes are compared with those of the free ligands in order to determine the coordination sites that may involved in chelation. The strong bands located at 1578 and 1586 cm^{-1} are assigned to the ν(C=N) stretching vibrations of pyridyl nitrogen of the H_2L^1 and H_2L^2 ligands.

Table 4. IR data (4000-400 cm^{-1}) of H_2L^1 ligand and its metal complexes*.

Compound	ν(OH) (hydrated water)	Y(S-H)	ν(C=N) (azomethine)	ν(C=N) (pyridine)	υ(C-S) (symm.)	ν(C-S) (asymm.)	δ(C=N) (pyridine)	ν(M-O) (coord. water)	ν(M-N)
H_2L^1	-	2370m	1612sh	1578sh	751sh	699sh	647m	-	-
$[Cr(H_2L^1)(H_2O)_3]Cl_3$	3379s	2390sh	1607sh	1555sh	762sh	680sh	680m	516m	450m
$[Mn(H_2L^1)Cl_2]\cdot 2H_2O$	Disapp	2400sh	1595sh	1562br	764sh	720sh	654m	Disapp.	419m
$[Fe(H_2L^1)(H_2O)_3]Cl_3\cdot H_2O$	3378br	2375sh	1651br	1617sh	763sh	681sh	625m	597m	430m
$[Co(H_2L^1)Cl_2]\cdot H_2O$	Disapp	2371sh	1612sh	1584sh	765sh	731sh	674m	Disapp.	425m
$[Ni(H_2L^1)Cl_2]\cdot H_2O$	Disapp	Disapp	1605sh	1550sh	762sh	675sh	675m	Disapp.	423m
$Cu(H_2L^1)Cl_2]\cdot 4H_2O$	Disapp	2369sh	1619sh	1578sh	765sh	735sh	685m	Disapp.	424m
$[Cd(H_2L^1)Cl_2]\cdot 4H_2O$	Disapp	2342sh	1609sh	1609sh	762sh	710sh	660m	Disapp.	450m
$[UO_2(H_2L^1)(CH_3COO)_2]\cdot H_2O$	Disapp	2373s	1608br	1566sh	755sh	730sh	667m	548m	413m

*sh = sharp, m = medium, br = broad, s = small, w = weak.

Table 5. IR data (4000-400 cm^{-1}) of H_2L^2 ligand and its metal complexes*.

Compound	ν(OH) (carboxylic	υ(C=O) (carboxylic	ν(C=N) (azomethine)	ν(C=N) (pyridine)	υ(COO) (asym.)	υ(COO) (sym.)	δ(C=N) (pyridine)	υ(M-O) (carboxylic)	υ(M-N)
H_2L^2	3374sh	1740w	1618sh	1586sh	1586sh	1485	656m	-	-
$[Cr(H_2L^2)Cl_3]\cdot 3H_2O$	3403br	1750w	1691br	1627br	1521s	1397sh	686sh	562w	446s
$[Mn(H_2L^2)(H_2O)Cl_2]\cdot 3H_2O$	3403sh	1745sh	1591sh	1593sh	1591sh	1390s	689br	530s	425s
$[Fe(H_2L^2)Cl_3]$	3400br	Disapp	1627br	1585sh	1564s	1418s	656sh	554s	418s
$[Co(H_2L^2)Cl_2]\cdot 2H_2O$	3421br	1705sh	1622sh	1570sh	1570s	1390sh	685br	535w	433s
$[Ni(H_2L^2)Cl_2]\cdot 4H_2O$	3422br	1718sh	1628sh	1569sh	1569s	1392sh	685m	561br	424s
$[Cu(H_2L^2)Cl_2]\cdot 3H_2O$	3404sh	1740w	1626sh	1554sh	1554sh	1471sh	686sh	526s	422s
$[Cd(H_2L^2)Cl_2]\cdot 3H_2O$	3336br	1715sh	1618sh	1583br	1587s	1384sh	650m	530s	432s
$[Th(H_2L^2)Cl_3]Cl$	3404br	Disapp	1625	1557br	1557s	1387sh	688m	525s	421s
$[UO_2(H_2L^2)(CH_3COO)_2]\cdot H_2O$	3436br	Disapp	1607br	1567sh	1567sh	1360sh	689br	542w	445s

*sh = sharp, m = medium, br = broad, s = small, w = weak.

These bands are shifted to 1550-1617 and 1554-1627 cm^{-1} for H_2L^1 and H_2L^2 metal complexes, respectively [14]. The sharp IR ligand bands at 647 and 656 cm^{-1} are assigned to the δ(C=N) of pyridine for H_2L^1, and H_2L^2 ligands, respectively [14]. These bands are shifted to 650-680, and 650-689 for H_2L^1, and H_2L^2 metal complexes, respectively. The strong and sharp band of υ(C=N) stretching vibration of the azomethine is found at 1612 and 1618 cm^{-1} for H_2L^1 and H_2L^2, respectively. These bands are found at 1595-1651 and 1591-1691 cm^{-1} in the H_2L^1 and H_2L^2 complexes, respectively, indicating the participation of the azomethine nitrogen in coordination (M-N) [13,14,35,36]. The υ(OH), υ(C=O), υ_{asym}(COO) and υ_{sym}(COO) stretching vibrations of the carboxylate O are observed at 3374, 1740, 1586 and 1485 cm^{-1} for H_2L^2 ligand, respectively. These stretching vibrations are disappeared or shifted to higher or lower frequencies at 3336-3422, 1705-1750, 1521-1591 and 1360-1471 cm^{-1} for H_2L^2-metal complexes. These blue or red shifts may attribute to hydrogen bond formation [13,14]. The SH, υ_{sym}(CS) and υ_{sym}(CS) stretching vibrations are observed at 2370, 699 and 751 cm^{-1} for H_2L^1 ligand, respectively. While in complexes, these bands are disappeared or shifted to lower or higher wavenumbers in the spectra at 2342-2400, 675-735 and 755-765 cm^{-1} for H_2L^1 complexes may attributed to hydrogen bond formation [13,14]. New bands are found in the spectra of the complexes in the regions 516-597 (coordinated water O), and 530-542 (coordinate water and AcO) which are assigned to υ(M-O) stretching vibrations for H_2L^1 and H_2L^2 metal complexes, respectively. The bands at 413-450 and 418-446 cm^{-1} for H_2L^1 and H_2L^2 metal complexes, respectively, have been assigned to υ(M-N) mode [14,37]. Therefore, from the IR spectra, it is concluded that H_2L^1 and H_2L^2 ligands behave as neutral tridentate ligands and bind to the metal ions via the two azomethine N and pyridine N.

The other series of weak bands between 3100 and 2800 cm^{-1} are related to (C H) modes of vibrations. Also, some weak bands located between 2000 and 1750 cm^{-1} can be assigned to overtones of the aromatic rings. The shift to higher or lower wavenumbers can be attributed to important hydrogen bonding effects [12-14,37]. Most of the band shifts observed at the wave number region 1150-994 cm^{-1} are in agreement with the structural changes observed in the molecular carbon skeleton after complexation, which cause some important changes in (C-C) bond lengths.

3.9. ^{1}H NMR spectra

The NMR spectra of Schiff base and its Cd(II) complex are recorded in dimethylsulphoxide (DMSO-d_6) solution using tetramethylsilane (TMS) as an internal standard. The spectrum of the complex is examined in comparison with those of the parent Schiff base. Upon examinations it is found that the SH signal, appeared in the spectrum of H_2L^1 ligand at 4.03 ppm, is found in the spectrum of its Cd(II) complex at 4.10 ppm indicating that the SH proton is not participated in the chelation with metal ion. The COOH signal is found at 13.45 ppm in the spectrum of H_2L^2 ligand. This signal is deshielded at 13.40 ppm of Cd(II) complex. This indicates the non-involvement of the COOH group in chelation while its involvement in hydrogen bond formation.

3.10. Magnetic susceptibility and electronic spectral studies

The diffused reflectance spectra of Cr(III) chelates for H_2L^1 and H_2L^2 ligands exhibit bands at 21,047-23,741 which may be assigned to the $^6A_{1g} \rightarrow {}^4T_{2g}$ (G) transition in octahedral geometry of the complexes [38]. The $^6A_{1g} \rightarrow {}^5T_{1g}$ transition appears to be split into two bands at 15,348-16,452 cm^{-1}. The observed magnetic moments of Cr(III) complexes are 4.12 and 4.42 B.M. Thus, the complexes formed have the octahedral geometry involving sp^3d^2 hybridization [15]. The spectra also show bands at 24,721-25,641 cm^{-1} which may be attributed to ligand-metal charge transfer. While spectra of the Mn(II) complexes show three bands at 15,378-16,025, 21,839-22,056 and 26,577-27,330 cm^{-1} assignable to $^4T_{1g} \rightarrow {}^6A_{1g}$, $^4T_{2g}(G) \rightarrow {}^6A_{1g}$ and $^4T_{1g}(D) \rightarrow {}^6A_{1g}$ transitions, respectively [39]. The magnetic moment values are 4.80, and 3.01 B.M. for Mn-H_2L^1, and Mn-H_2L^2 complexes, respectively, which indicate the presence of Mn(II) ions in octahedral structure for $H_2L^1$and in triagonal bipyramidal in H_2L^2. From the diffused reflectance spectra it is observed that, the Fe(III) chelates exhibit bands at 21,491-22,026 cm^{-1} which may be assigned to the $^6A_{1g} \rightarrow {}^4T_{2g}$ (G) transition in octahedral geometry [38,15].

Table 6. Thermoanalytical results (TG, DTG and DTA) of H_2L^1 ligand and its metal complexes.

Complex	TG range (°C)	DTG_{max} (°C)	Peak temp. In DTA (°C)	n*	Total mass loss Estim (Calcd)%	Assignment	Metallic residue
H_2L^1	180-390	225		1	39.34 (39.00)	- Loss of C_7H_6NS.	-
	390-580	400		1	32.41 (33.23)	- Loss of $C_7H_4N_2$.	
	580-1000	780		1	28.25 (27.80)	- Loss of C_5H_5S.	
					100.0 (100.0)		
$[Fe(H_2L^1)(H_2O)_3]Cl_3{\cdot}H_2O$	30-160	70, 140	60(+), 130(-)	2	8.94 (9.68)	- Loss of H_2O and HCl.	½ Fe_2O_3
	160-450	390	260(+), 610(+)	1	32.13 (31.15)	- Loss of C_6H_4S.	
	450-640	600		1	46.68 (47.50)	- Loss of $C_{13}H_{12}N_3SO_{1.5}$.	
					87.75 (88.03)		
$[UO_2(H_2L^1)(CH_3COO)_2]{\cdot}H_2O$	30-350	73, 180	50(+), 250(+),	3	16.14 (16.48)	- Loss of H_2O, $2CO_2$ and C_2H_6.	UO_2
	350-500	400	420(-), 580(+)	1	17.06 (16.36)	- Loss of C_7H_5NS.	
	500-675	550		1	24.86 (25.45)	- Loss of $C_{12}H_6N_2S$.	
					58.06 (58.29)		
$[Co(H_2L^1)Cl_2]{\cdot}H_2O$	30-160	78, 190	50(+), 180(+),	2	29.95 (29.70)	- Loss of 2HCl and C_6H_6S.	CoO
	160-370	240	250(+), 630(+)	1	43.65 (44.45)	- Loss of 2HCl and $C_{12}H_3N_3S$.	
	370-670	550		1	3.44 (3.23)	- Loss of CH_4.	
					77.04 (77.38)		
$[Cr(H_2L^1)(H_2O)_3]Cl_3$	30-230	75	60(+), 220(+),	1	20.67 (20.22)	- Loss of 3HCl.	½ Cr_2O_3
	230-450	290	580(-)	1	31.27 (31.94)	- Loss of $C_9H_5N_2S$.	
	450-650	580		1	33.39 (33.61)	- Loss of $C_{10}H_8NSO_{0.5}$.	
					85.33 (85.77)		

n* = number of decomposition steps. (+) = Endothermic and (-) = Exothermic.

The $^6A_{1g} \rightarrow {}^5T_{1g}$ transition appears to be split into two bands at 11,742-12,782 cm^{-1}. The magnetic moment values of Fe(III) complexes are found to be 5.83 and 5.51 B.M. for H_2L^1 and H_2L^2 ligands, respectively, which indicates the presence of both complexes in octahedral geometry [38]. The spectra show also bands at 24,641-25,510 cm^{-1} which may attribute to ligand - metal charge transfer. The diffused reflectance spectra of Co(II) complexes of H_2L^1 and H_2L^2 ligands resemble those of other five coordinate Co(II) complexes, where three bands are observed at 12,752-12,874, 15,542-15,671 and 17,491-17,514 cm^{-1}. The fourth band at 21,771-23,312 cm^{-1} refers to the charge transfer band. The low magnetic moment values (μ_{eff} = 4.39-4.91 B.M.) compared with those observed for octahedral or tetrahedral complexes may support the five coordinate geometry [12-14]. The diffused reflectance spectra of the Ni(II) complexes show recognizable spectral bands at 13,470-23,984 cm^{-1}. The positions of these spectral bands are quite consistent with those predicted for five coordinate Ni(II) complexes [12-14]. The bands can be assigned, respectively, to $^3B_1 \rightarrow {}^3E$, $^3B_1 \rightarrow {}^3A_2$ and $^3B_1 \rightarrow {}^3E$ transitions assuming the effective symmetry to be C_{4V}. The bands at 27,560 and 27,457 cm^{-1}, for Ni (II) complexes with H_2L^1 and H_2L^2, respectively, may assigned to L $\rightarrow$ MCT band. The reflectance spectra of Cu (II) complexes of H_2L^1 and H_2L^2 ligands exhibit broad bands at 12,578-12,914, 15,612-16,001 and 19,214-19,874 cm^{-1}. These bands are generally consistent with a five coordinate geometry for Cu(II) complexes [12-14,38]. The spectra also show a band at 30,140-30,610 cm^{-1} which may assign to L-MCT band. The magnetic moment values of 2.01 and 1.96 B.M. for Cu (II)-H_2L^1 and Cu (II)-H_2L^2, respectively, are indicative of trigonal bipyramidal structure [12-14]. The complexes of Cd(II) and UO_2(II) are diamagnetic. According to the empirical formulae of these complexes, trigonal bipyramidal geometry is proposed. According to the empirical formula, Th(IV) complex is proposed to have octahedral.

3.11. Thermal analyses (TG, DTG and DTA) of Schiff bases

The TG curve of Schiff base H_2L^1 exhibits a first estimated mass loss of 39.34% (calcd. 39.00%) at 180-390 °C, which may be attributed to the elimination of C_7H_6NS molecule as gases (Table 6). In the second estimated mass loss of 32.41% (calc. 33.23%), at 390-580 °C, which may be attributed to the liberation of $C_7H_4N_2$ molecule. In the 3rd stages within the temperature range from 580 to 1000 °C, H_2L^1 loss the remaining part with an estimated mass loss of 28.25% (calcd. 27.80%) with a complete decomposition as gases. The Schiff base H_2L^2 decomposed in two stages (Table 7). From 30-250 °C, this step exhibits estimated mass loss of 64.38% (calcd. 64.88%), which may be attributed to the liberation of $C_{14}H_{10}O_4$ as gases. In the second step at temperature ranges from 250-970 °C it involve mass loss of 35.62% (calcd. 35.12%), which may be attributed to the liberation of $C_7H_5N_3$ molecule and corresponds to the complete decomposition of H_2L^2 as deduced from mass loss calculation (found mass loss = 100.0 %, calcd. mass loss = 100.0 %).

3.12. Thermal analyses (TG, DTG and DTA) of the metal chelates

Fe(III)-H_2L^1 and Fe(III)H_2L^2 chelates exhibit four steps of decomposition within the temperature range from 30-640 and 30-650 °C, respectively. For Fe(III)-H_2L^1 complex (Table 6), the first two steps of decomposition occur within the temperature range from 30-160 °C in which dehydration of water molecule and HCl gases occur with an estimated mass loss of 8.94% (calcd. 9.68%). The third step within the temperature range 160-450 °C, involves liberation of C_6H_4S molecule with an estimated mass loss of 32.13% (calcd. 31.15%). In the final step, liberation of $C_{13}H_{12}N_3SO_{1.5}$ molecule occurs with estimated mass loss of 46.68% (calcd. 47.50%) within the temperature range 450-640 °C. While for Fe(III)-H_2L^2 chelate (Table 7), the first step of decomposition occurs within the temperature rang 30-120 °C with an estimated mass loss of 6.51% (calcd. 6.82%) which can attributed to the loss of HCl gas. In the two successive decomposition steps within the temperature range 120-440 °C, liberation of HCl gas and $C_7H_4O_2$ molecule takes place with an estimated mass loss of 36.24% (calcd. 36.07%). In the final step, the estimated mass loss of 41.90% (calcd. 42.24%) may be attributed to the liberation of $C_{14}H_8N_3O_{0.5}$ molecule within the temperature range from 440-650 °C.

For UO_2(II)-H_2L^1 chelate, the first three steps of decomposition involve the loss of hydrated water molecule, $2CO_2$ and C_2H_6 with an estimated mass loss of 16.14% (calcd. 16.48%) within temperature range 30-350 °C (Table 6). The fourth step within the temperature range 350-500 °C in which liberation C_7H_5NS occurs with an estimated mass loss of 17.06 % (calcd. 16.36%) is observed. In the final step, an estimated mass loss of 24.76% (calcd. 25.45%) can be accounted for the loss of $C_{12}H_6N_2S$ molecule.

Table 7. Thermoanalytical results (TG, DTG and DTA) of H_2L^2 ligand and its metal complexes.

Complex	TG range (°C)	DTG_{max} (°C)	Peak temp. In DTA (°C)	n*	Total mass loss Estim (Calcd)%	Assignment	Metallic residue
H_2L^2	30-250	75		1	64.38 (64.88)	- Loss of $C_{14}H_{10}O_4$.	-
	250-970	610		1	35.62 (35.12)	- Loss of $C_7H_5N_3$.	
					100.0 (100.0)		
$[Fe(H_2L^2)Cl_3]$	30-120	85	80(+), 180(+),	1	6.51 (6.82)	- Loss of HCl.	½ Fe_2O_3
	120-440	180, 410	420(-), 600(+)	2	36.24 (36.07)	- Loss of HCl and $C_7H_4O_2$.	
	440-650	520		1	41.90 (42.24)	- Loss of $C_{14}H_8N_3O_{0.5}$.	
					84.64 (85.13)		
$[UO_2(H_2L^2)(CH_3COO)_2].H_2O$	30-220	60, 180	70(+), 180(+),	2	9.09 (9.05)	- Loss of H_2O, O_2 and C_2H_3.	UO_2
	220- 460	275, 410	250(-), 440(+),	2	19.82 (21.03)	- Loss of $2CO_2$ and C_7H_7.	
	460-950	650	600(-)	1	30.44 (29.73)	- Loss of $C_{14}H_{11}O_2N_3$.	
					59.35 (59.81)		
$[Co(H_2L^2)Cl_2].2H_2O$	60-220	99-199	80(+), 210(-),	2	16. 63 (16.88)	- Loss of HCl and H_2O.	CoO
	220	410	430(+), 590(-)	1	39.50 (39.29)	- Loss of $C_{12}H_7O_2N$.	
	450	630		1	32.24 (32.65)	- Loss of $C_9H_8O_2N_2$.	
	450-820				88.37 (88.82)		
$[Cr(H_2L^2)Cl_3].3H_2O$	30-140	94	80(+), 180(+),	1	9.53 (9.22)	- Loss of $3H_2O$.	$^1/_2$ Cr_2O_3
	140-450	190, 350	410(-), 590 (+)	2	41.68 (41.59)	- Loss of 3HCl and $C_7H_4NO_2$.	
	450-850	650		1	36.07 (36.21)	- Loss of $C_{14}H_8N_2O_{0.5}$.	
					87.28 (87.02)		

n* = number of decomposition steps. (+) = Endothermic and (-) = Exothermic.

From data listed in Table 7, it is clear that UO_2(II)-H_2L^2 chelat, the first two steps within the temperature range 30-220 °C may be attributed to loss of water and O_2 as gases and C_2H_3 molecule with an estimated mass loss 9.09% (calcd. 9.05%). The subsequent steps (220-950 °C) correspond to removal of organic part of ligand leaving metal oxide as a residue.

Co(II)-H_2L^1 chelate shows four decomposition steps within the temperature range 30-670 °C. The first two steps are found to correspond to loss of 2HCl and C_6H_6S with an estimated mass loss of 29.95% (calcd. 29.70%) in the temperature range from 30 to 160 °C (Table 6). The subsequent 3rd and 4th steps within the temperature range 160-670 °C are corresponding to removal of the organic part of the ligand and leaving metal oxide as residue. The data listed in Table 7 show that Co(II)-H_2L^2 chelat has four steps of decomposition within the temperature range from 60-820 °C. The first two steps involve the loss of one water molecule and HCl gas with estimated mass loss of 16.63% (calcd. 16.88%) within the temperature range from 60-220°C. The other two subsequent steps in the temperature range 220-820 °C involve the loss of the remaining part of the ligand leaving metal oxide residue. The TG curves of the Cr(III)-chelates, show three to five stages of decomposition within the temperature range of 30-1000 °C with total mass loss of 85.33% (calcd. 85.77%) and 87.28% (calcd. 87.02%) for Cr(III)-H_2L^1 and Cr(III)-H_2L^2 chelates, respectively, (Tables 6 and 7). In all steps, decomposition of the ligand occurred and residues of metal oxide are left.

The decomposition steps of these complexes are accompanied by the appearance of endothermic and exothermic peaks through all stages of decomposition as shown in Tables 6 and 7.

3.13. Calculation of activation thermodynamic parameters

The thermodynamic activation parameters of decomposition processes of dehydrated complexes namely activation energy (E*), enthalpy (ΔH*), entropy (ΔS*) and Gibbs free energy change of the decomposition (ΔG*) are evaluated graphically by employing the Coats-Redfern relation [40] and the data are summarized in Tables 8 and 9.

$$\log\left[\frac{\log\{W_f/(W_f-W)\}}{T^2}\right] = \log\left[\frac{AR}{\theta E^*}\left(1-\frac{2RT}{E^*}\right)\right] - \frac{E^*}{2.303\,RT} \quad (1)$$

where W_f is the mass loss at the completion of the reaction, W is the mass loss up to temperature T; R is the gas constant, E* is the activation energy in kJ/mol, θ is the heating rate and (1-(2RT/E*)) ≅ 1. A plot of the left-hand side of equation (1) against 1/T gives a slope from which E* is calculated and A (Arrhenius factor) is determined from the intercept. The entropy of activation (ΔS*), enthalpy of activation (ΔH*) and the free energy change of activation (ΔG*) are calculated using the following equations:

$$\Delta S^* = 2.303\,[\log(Ah/kT)]R \quad (2)$$

$$\Delta H^* = E^* - RT \quad (3)$$

$$\Delta G^* = \Delta H^* - T\Delta S^* \quad (4)$$

The activation energies of decomposition are found to be in the range from 30.77 to 250.8 kJ/mol. The high values of the activation energies reflect the thermal stability of the complexes. The entropy of activation is found to have negative values in all the complexes which indicate that the decomposition reactions proceed with a lower rate than the normal ones or the decomposition process occurs spontaneously.

3.14. Structural interpretation

The suggested structures of the complexes of Schiff bases; H_2L^1 and H_2L^2, with Cr(III), Mn(II), Fe(III), Co(II), Ni(II), Cu(II), Cd(II), Th(IV) and UO_2(II) ions are given in Figures 3 and 4.

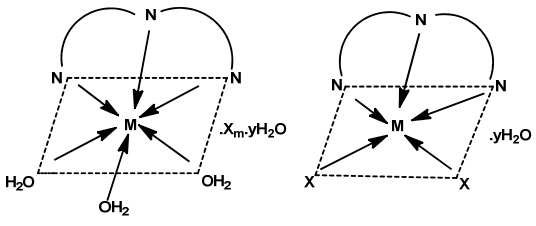

M= Cr(III), X= Cl, m=3, y=0
M= Mn(II), X= Cl, y=2
M= Fe(III), X= Cl, m=3, y=1
M= Co(II), X= Cl, y=1
M= Ni(II), X= Cl, y=1
M= Cu(II), X= Cl, y=4
M= Cd(II), X= Cl, y=4
M= UO_2(II), X= AcO, y=1

Figure 3. Structural formulae of H_2L^1 metal complexes.

Table 8. Thermodynamic data of the thermal decomposition of metal complexes of H_2L^1.

Complex	Decomp. Temp. (°C)	E*(CR) kJ/mol	A 1/s	ΔS* kJ/mol	ΔH* kJ/mol	ΔG* kJ/mol
$[Fe(H_2L^1)(H_2O)_3]Cl_3{\cdot}H_2O$	25-190	57.6	1.25×10^{16}	-39.3	57.05	59.7
	190-395	40.2	1.07×10^{7}	-106.4	38.69	58.4
	395-520	27.9	2.57×10^{6}	-121.2	25.59	57.5
	520-650	41.9	1.52×10^{6}	-131.9	37.17	111.5
$[UO_2(H_2L^1)(CH_3COO)_2]{\cdot}H_2O$	25-245	34.8	7.71×10^{5}	-126.2	33.60	51.9
	245-420	28.7	4.61×10^{6}	-115.8	26.69	55.2
	420-580	66.1	3.16×10^{6}	-123.6	62.54	116.1
	580-680	66.1	1.46×10^{6}	-132.2	61.46	135.5
$[Co(H_2L^1)\ Cl_2]{\cdot}H_2O$	28-195	46.4	6.35×10^{4}	-145.4	45.42	62.8
	195-300	60.3	1.09×10^{7}	-109.4	58.01	87.6
	300-570	173.5	3.54×10^{11}	-27.5	169.60	182.3
	570-690	234.1	2.90×10^{5}	-145.7	229.40	312.5
$[Cr(H_2L^1)(H_2O)_3]Cl_3$	25-185	41.3	8.21×10^{4}	-142.7	40.37	56.3
	185-260	60.3	1.92×10^{7}	-101.7	58.70	77.91
	260-450	82.6	8.54×10^{6}	-113.5	79.75	118.9
	450-610	86.5	1.46×10^{5}	-151.3	81.80	166.6

Table 9. Thermodynamic data of the thermal decomposition of metal complexes of H_2L^2.

Complex	Decomp. Temp. (°C)	E*(CR) kJ/mol	A 1/s	ΔS* kJ/mol	ΔH* kJ/mol	ΔG* kJ/mol
$[Fe(H_2L^2)Cl_3]$	30-120	56.5	2.60×10^{7}	-92.7	55.8	63.9
	120-180	86.3	9.14×10^{8}	-69.4	84.8	97.5
	180-410	144.8	1.39×10^{10}	-53.5	141.3	163.5
	410-620	136.5	3.55×10^{6}	-124.3	132.1	197.6
$[UO_2(H_2L^2)(CH_3COO)_2]{\cdot}H_2O$	30-160	28.2	7.72×10^{6}	-108.1	26.8	44.5
	160-320	181.3	6.24×10^{7}	-94.4	179.2	203.3
	320-440	212.8	3.66×10^{9}	-62.5	209.6	229.8
	440-600	105.0	4.47×10^{6}	-120.9	101.3	154.7
$[Co(H_2L^2)Cl_2]{\cdot}2H_2O$	30-100	72.0	1.63×10^{9}	-59.1	71.2	76.8
	100-199	79.7	2.34×10^{7}	-100.7	77.9	98.4
	199-380	66.3	6.86×10^{6}	-112.9	64.1	93.4
	380- 520	210.0	7.76×10^{6}	-116.7	206.2	260.2
$[Cr(H_2L^2)Cl_3]{\cdot}3H_2O$	30-90	239.3	4.14×10^{9}	-151.2	238.5	243.3
	90-210	58.6	1.90×10^{5}	-140.4	57.0	84.5
	210-450	185.6	3.21×10^{9}	-64.9	182.4	206.9
	450-620	250.8	4.22×10^{12}	-6.8	247.0	250.1

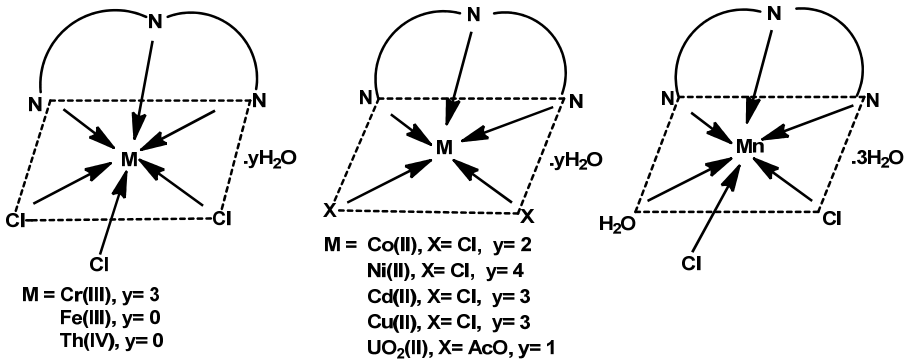

Figure 4. Structural formulae of H_2L^2 metal complexes.

3.15. Biological activity

In testing the antibacterial and antifungal activity of these compounds we used more than one test organism to increase the chance of detecting antibiotic principles in tested materials. The sensitivity of a microorganism to antibiotics and other antimicrobial agents was determined by the assay plates which incubated at 28 °C for two days for yeasts and at 37 °C for one day for bacteria. All of the tested compounds showed a remarkable biological activity against different types of Gram-positive (*Bacillus Subtilis* ATTC 6051 and *S. pyogones* ATTC 12600) and Gram-negative bacteria (*Escherichia Coli* ATTC 11775 and *Proteus Vulgaris* ATTC 13315) and *Fusarium Solani Martius* and *Aspergillus Niger* Fungus. The data are listed in Tables 10 and 11. On comparing the biological activity of the Schiff bases and their metal complexes, the following results are obtained:

Bacteria: H_2L^1 ligand is found to have no biological activity against all tested bacteria. But metal complexes are found to have sensitivity for inhibition of Gram-positive more than Gram-negative bacteria. According to the data listed in Table 10, biological activity of metal complexes are found to follow the order Co(II) > Cd(II) > Cr(III) > Fe(III) > Ni(II) > Mn(II) > UO_2(II) for Gram-positive and Ni(II) ≈ Fe(III) > Cd(II) > Co(II) > Mn(II) > UO_2(II) > Cr(III) for Gram-negative bacteria. But Cu (II) complex do not show any antibacterial activity. Therefore, it is concluded that the present of metal ions as the result of complexation enhance the biological activity of the parent Schiff base.

Table 10. Biological activity and MIC_{50} of H_2L^1 ligand and its metal complexes.

Sample	Fungus		Bacteria			
			G. -ve		G. +ve	
	F. Solani	*A. Niger*	*E. Coli*	*P. Vulgaris*	*B. Subtilis*	*S. Pyogones*
H_2L^1	1.1	0.9	-ve	-ve	-ve	-ve
MIC_{50}	>100 µg/mL	>100 µg/mL	-ve	-ve	-ve	-ve
$[Cr(H_2L^1)(H_2O)_3]Cl_3$	2.1	2.6	2.2	2.3	3.4	3.2
MIC_{50}	>100 µg/mL	>100 µg/mL	>100 µg/mL	>100 µg/mL	50 µg/mL	50 µg/mL
$[Mn(H_2L^1)Cl_2]\cdot 2H_2O$	1.3	1.8	2.7	2.6	2.9	2.7
MIC_{50}	>100 µg/mL	>100 µg/mL	>100 µg/mL	>100 µg/mL	50 µg/mL	>100 µg/mL
$[Fe(H_2L^1)(H_2O)_3]Cl_3\cdot H_2O$	1.5	1.7	2.9	3.1	3.3	3.1
MIC_{50}	>100 µg/mL	>100 µg/mL	50 µg/mL	50 µg/mL	50 µg/mL	50 µg/mL
$[Co(H_2L^1)Cl_2]\ H_2O$	2.0	2.3	2.8	2.9	3.8	3.7
MIC_{50}	>100 µg/mL	>100 µg/mL	50 µg/mL	50 µg/mL	25 µg/mL	25 µg/mL
$[Ni(H_2L^1)Cl_2]\cdot H_2O$	2	2.1	2.9	3.1	3.2	3.2
MIC_{50}	>100 µg/mL	>100 µg/mL	50 µg/mL	50 µg/mL	50 µg/mL	50 µg/mL
$Cu(H_2L^1)Cl_2]\cdot 4H_2O$	3.0	3.0	-ve	-ve	-ve	-ve
MIC_{50}	50 µg/mL	50 µg/mL	-ve	-ve	-ve	-ve
$[Cd(H_2L^1)Cl_2]\ .4H_2O$	5.0	4.5	2.9	2.8	3.6	3.4
MIC_{50}	12.5 µg/mL	25 µg/mL	50 µg/mL	50 µg/mL	50 µg/mL	50 µg/mL
$[UO_2(H_2L^1)(CH_3COO)_2].H_2O$	0.5	0.9	2.3	2.5	2.6	2.4
MIC_{50}	>100 µg/mL	>100 µg/mL	>100 µg/mL	>100 µg/mL	>100 µg/mL	>100 µg/mL

Table 11. Biological activity of H_2L^2 ligand and its metal complexes.

Sample	Fungus		Bacteria			
			G. -ve		G. +ve	
	A. Nigar	*A. Llavus*	*E. Coli*	*P. Vulgaris*	*B. Subtilis*	*S. Pyogones*
H_2L^2	2.0	1.8	2.2	2.1	2.2	2.0
MIC_{50}	>100 µg/mL	>100 µg/mL	>100 µg/mL	>100 µg/mL	>100 µg/mL	>100 µg/mL
$[Cr(H_2L^2)Cl_3].3H_2O$	-ve	-ve	2.1	2.0	0.9	0.7
MIC_{50}	-ve	-ve	>100 µg/mL	>100 µg/mL	>100 µg/mL	>100 µg/mL
$[Mn(H_2L^2)(H_2O)Cl_2].3H_2O$	-ve	-ve	1.9	1.8	2.3	2.3
MIC_{50}	-ve	-ve	>100 µg/mL	>100 µg/mL	>100 µg/mL	>100 µg/mL
$[Fe(H_2L^2)Cl_3]$	-ve	-ve	1.3	1.0	1.4	1.1
MIC_{50}	-ve	-ve	>100 µg/mL	>100 µg/mL	>100 µg/mL	>100 µg/mL
$[Co(H_2L^2)Cl_2].2H_2O$	-ve	-ve	3.0	2.9	2.0	2.2
MIC_{50}	-ve	-ve	50 µg/mL	50 µg/mL	>100 µg/mL	>100 µg/mL
$[Ni(H_2L^2)Cl_2].4H_2O$	-ve	-ve	2.8	2.4	3.2	3.1
MIC_{50}	-ve	-ve	>100 µg/mL	>100 µg/mL	>100 µg/mL	5o µg/mL
$[Cu(H_2L^2)Cl_2].3H_2O$	0.7	0.5	1.2	1.0	2.0	1.8
MIC_{50}	>100 µg/mL	>100 µg/mL	>100 µg/mL	>100 µg/mL	>100 µg/mL	>100 µg/mL
$[Cd(H_2L^2)Cl_2].3H_2O$	2.5	2.7	1.7	1.6	2.1	1.7
MIC_{50}	>100 µg/mL	>100 µg/mL	>100 µg/mL	>100 µg/mL	>100 µg/mL	>100 µg/mL
$[Th(H_2L^2)Cl_3].Cl$	-ve	-ve	2.2	2.0	2.1	2.0
MIC_{50}	-ve	-ve	>100 µg/mL	>100 µg/mL	>100 µg/mL	>100 µg/mL
$[UO_2(H_2L^2)(CH_3COO)_2].H_2O$	-ve	-ve	-ve	-ve	-ve	-ve
MIC_{50}	-ve	-ve	-ve	-ve	-ve	-ve

Fungus: Schiff base H_2L^1 ligand shows antifungal activity against *F. Solani* and A*. Niger*. From Table 10, H_2L^1 is found to have high sensitivity against *F. Solani* than *A. Niger*. Metal complexes have antifungal biological activity and follow the order Cd(II) > Cu(II) > Cr(III) > Co(II) > Ni(II) > Fe(III) > Mn(II) > UO_2(II). It is also clear from Table 10 that the Cr (III), Mn(II), Fe(III), Co(II), Ni(II), Cu(II) and Cd(II) complexes are found to have antifungal activity more than the parent H_2L^1 ligand.

Bacteria: Biological activity of H_2L^2 ligand and its metal complexes are given in Table 11. Schiff base H_2L^2 is found to inhibit all tested bacteria at different rates. Sensitivity of Schiff base H_2L^2 toward the organisms has follow the order *B. Subtilis* > *S. Pyogones* for Gram-positive and *E. Coli* > *P. Vulgaris* for Gram negative. Metal complexes are also found to inhibit all the tested bacteria at different rates. Sensitivity of metal complexes towards organisms are found to follow the order Ni(II) > Mn(II) > Co(II) > Th(IV) > Cu(II) > Cd(II) > Fe(III) > Cr(III) for Gram-positive and Co(II) > Ni(II) > Th(IV) > Cr(III) > Mn(II) > Cd(II) Fe(III) > Cu(II) for Gram-negative bacteria. But UO_2 (II) does not have any antibacterial activity. Co(II) and Ni(II) complexes are found to have antibacterial activity against Gram positive and Gram negative organisms more than the parent Schiff base, while Cr(III) and Th(IV) are found to have nearly the same biological activity. In addition, Mn(II) and Ni(II) complexes show higher biological activity against Gram positive bacteria more than the parent Schiff base (H_2L^2) (Table 11).

Fungus: Schiff base H_2L^2 shows antifungal activity against *A. Nigar* and *A. Llavus*. It has sensitivity toward the organisms in the following order *A. Nigar* > *A. Llavus*. But some metal complexes showed antifungal and sensitivity of these complexes toward organisms follow the order Cd(II) > Cu(II) and another metal complexes show any antifungal activity. The Cd(II) complex found to have antifungal activity higher than parent Schiff base (Table 11).

It was demonstrated that the Schiff base and its metal complexes showed a higher effect on *B. Subtilis* and *S. Pyogones* (Gram positive bacteria) than *P. Vulgaris* and *Escherichia coli* (Gram-negative bacteria). It is known that the membrane of Gram-negative bacteria is surrounded by an outer membrane containing lipopolysaccharides. The newly synthesized Schiff base and its metal complexes seem to be able to combine with the lipophilic layer in order to enhance the membrane permeability of the Gram-negative bacteria. The lipid membrane surrounding the cell favours the passage of only lipid soluble materials; thus the lipophilicity is an important factor that controls the antimicrobial activity. Also the increase in lipophilicity enhances the penetration of Schiff base and its metal complexes into the lipid membranes and thus restricts further growth of the organism [41,42]. This could be explained

by the charge transfer interaction between the studied molecules and the lipopolysaccharide molecules which lead to the loss of permeability barrier activity of the membrane. The Schiff base and its metal complexes could enhance the antimicrobial effect on both strains probably by the pyridyl and azomethine nitrogens and thiol group [43]. The Schiff base and its metal complexes are more toxic on *B. Subtilis* and *S. Pyogones* than on *Escherichia coli*, probably due to the thiol, COOH, S and phenyl groups, which might interact with the double membrane.

The activities of all the tested complexes may be explained on the basis of chelation theory; chelation reduces the polarity of the metal atom mainly because of partial sharing of its positive charge with the donor groups and possible p electron delocalization within the whole chelate ring. Also, chelation increases the lipophilic nature of the central atom which subsequently favors its permeation through the lipid layer of the cell membrane [44].

4. Conclusions

The results of this investigation support the suggested structures of the metal complexes. It is obvious from this study that only mononuclear complexes are obtained. Cr(III), Fe(III) and Th(IV) complexes have octahedral geometry while Co(II), Ni(II), Cu(II), Cd(II) and UO_2(II) complexes are trigonal bipyramidal except Mn(II) complexes, they have trigonal bipyramidal and octahedral geometry with H_2L^1 and H_2L^2, respectively. The biological activities of the Schiff bases under investigation and their complexes against bacterial and fungal organisms are promising which need further and deep studies on animals and humans.

References

[1]. Sima, J. *Crao. Chem. Acta* **2001**, *74*, 593-600.
[2]. Ouyang, X. M.; Fei, B. L.; Okamuro, T. A.; Sun, W. Y.; Tang, W. X.; Ueyama N. *Chem. Lett.* **2002**, *3*, 362-363.
[3]. Datta, A.; Karan, N. K.; Mitra, S.; Rosair, G. *Naturforsch. Z.* **2002**, *57b*, 999-1002.
[4]. Jayabalakrishnan, C.; Natarajan, K. *Trans. Met. Chem.* **2002**, *27*, 75-79.
[5]. Sharghi, H.; Nasseri, M. A. *Bull. Chem. Soc. Jpn*. **2003**, *76*, 137-142.
[6]. Lions, F.; Martin, F. K. V. *J. Am. Chem. Soc*. **1960**, *82*, 2733-2737.
[7]. Blake, A. J.; Lavery, A. J.; Hyde, T. I.; Schroder, M. *J. Chem. Soc. Dalton Trans*. **1989**, *5*, 965-970.
[8]. Curry, J. D.; Robinson, M. A.; Busch, D. H. *Inorg. Chem*. **1967**, *6*, 1570-1574.
[9]. Thabet, S. K.; Hagopian, L. *Mikrochim. Ichnoanal. Acta* **1965**, *5-6*, 964-965.
[10]. Yao, W.; Carbtree, R. H. *Inorg. Chem*. **1996**, *35*, 3007-3011.
[11]. Nugent, S. J.; Wang, Q. M.; Bruce, D. W. *New J. Chem*. **1996**, *20*, 669-675.
[12]. Vance, A. L.; Alcock, N. W.; Heppert, J. A.; Busch, D. H. *Inorg. Chem*. **1998**, *37*, 6912-6920.
[13]. Mohamed, G. G.; Abd El-Wahab, Z. H. *Spectrochim. Acta A* **2005**, *61*, 1059-1068.
[14]. Mohamed, G. G. *Spectrochim. Acta A* **2006**, *64*, 188-195.
[15]. Soliman, A. A.; Mohamed, G. G. *Thermochim. Acta* **2004**, *421*, 151-159.
[16]. Sarin, R.; Munshi, K. N. *J. Inorg. Nucl. Chem*. **1972**, *34*, 581-590.
[17]. Irving, H.; Rossotti, H. S. *J. Chem. Soc*. **1954**, *17*, 2904-2910.
[18]. Irving, H.; Rossotti, H. S. *J. Chem. Soc*. **1953**, *321*, 3397-3405.
[19]. Guerriero, P.; Bullita, F.; Vigato, P. A.; Pelli, B.; Traldi, P. *J. Heterocycl. Chem*. **1988**, *25(1)*, 145-154.
[20]. Bauer, A. W.; Kirby, W. M.; Sherris, C.; Turck, M. *Am. J. Clin. Path.* **1966**, *45*, 493-496.
[21]. Pfaller, M. A.; Burmeister, L.; Bartlett, M. A.; Rinaldi, M. G. *J. Clin. Microbiol.* **1988**, *26*, 1437-1441.
[22]. National Committee for Clinical Laboratory Standards. Antimicrobial susceptibilty of Flavobacteria. *Performance*, 41, 1997.
[23]. National Committee for Clinical Laboratory Standards. Methods for dilution antimicrobial susceptibility tests for bacteria that grow aerobically. Approved standard M7-A3, Villanova, PA, 1993.
[24]. National Committee for Clinical Laboratory Standards. Reference method for broth dilution antifungal susceptibilty testing of conidium-forming filamentous: proposed standard M38-A. Wayne, PA, USA, 2002.
[25]. National Committee for Clinical Laboratory Standards. Method for antifungal disc diffusion susceptibility testing of yeast: proposed guideline M44-P, Wayne, PA, USA, 2003.
[26]. Liebowitz, L. D.; Ashbee, H. R.; Evans, E. G. V.; Chong, Y.; Mallatova, N.; Zaidi, M.; Gibbs, D. and Global Surbeillance Group. Diagn. *Microbiol. Infect. Dis.* **2001**, *4*, 27-33.
[27]. Matar, M. J.; Zeichner, L. O.; Paetznick, V. L. J. R. Rodriguez, E. Chen, J. H. Rex. *Agents Chemother*. **2003**, *47*, 1647-1651.
[28]. Sari, N.; Arslan, S.; Logoglu, E.; Sakiyan, I. *J. Sci.* **2003**, *16*, 283-288.
[29]. Bjerrum, J.; Kgl. Metal Amine Formation in Aqueous Solution, Haase, Kopenhagen, 1941.
[30]. Irving, H.; Williams, R. J. P. *J. Chem. Soc*. **1953**, *8*, 3192-3210.
[31]. Olie, G. H.; Olive, S. The Chemistry of the Catalyzes Hydrogenation of Carbon Monoxide, Springer, Berlin, 1984. pp. 152
[32]. Orgel, L. E. An Introduction Metal Chemistry: Ligand Field Theory, 2nd Edn. , Chapt. 2, 3, 4, Methuen**, 1966.**
[33]. Blake, A. J.; Lavery, A.; Schroder, M. *Acta Crytallogr. C* **1996** *52*, 37-39.
[34]. Gemel, C.; Folting, K.; Caulton, K. G. *Inorg. Chem*. **2000**, *39*, 1593-1597.
[35]. Pernak, J.; Rogoza, J. *Arkivoc*. **2000**, *1*, 889-904.
[36]. Mohamed, G. G.; Omar, M. M.; Ibrahim, A. A. *Eur. J. Med. Chem*. **2009**, *44*, 4801-4812.
[37]. Nakamoto, K. Infrared and Raman Spectra of Inorganic and Coordination Compounds, fourth ed., Wiley, New York, 1980.
[38]. Cotton, F. A.; Wilkinson, G.; Murillo, C. A.; Bochmann, M. Advanced Inorganic Chemistry, 6th ed., Wiley, New York, 1999.
[39]. Sanmartin, J; Bermejo, M. R.; Deibe, A. M. G.; Maneiro, M.; Lage, C. Filho, A. J. C. *Polyhedron* **2000**, *19*, 185-192.
[40]. Coats, A. W.; Redfern, J. P. *Nature* **1964**, *201*, 68-69.
[41]. Tumer, M.; Koksal, H.; Sener, M. K. *Trans. Met. Chem*. **1999**, *24*, 414-420.
[42]. Imran, M.; Iqbal, J.; Iqbal, S.; Ijaz, N. *Turk. J. Biol.* **2007**, *31*, 67-72.
[43]. Azam, F.; Singh, S.; Khokhra, S. L.; Prakash, O. *J. Zhejiang Univ. Sci. B*. **2007**, *8*, 446-452.
[44]. Caudhary, A.; Singh, R. V. *Phosphorus Sulfur Silicon Relat. Elem*. **2003**, *178*, 603-613.